Available online at www.sciencedirect.com
SCIENCE DIRECT®
Polymer 45 (2004) 2017–2030
polymer
www.elsevier.com/locate/polymer

Experimental investigation of the governing parameters in the electrospinning of polymer solutions

S.A. Theron[a], E. Zussman[a,b,*], A.L.. Yarin[a,c]

[a]Faculty of Mechanical Engineering, Technion-Israel Institute of Technology, Haifa 32000, Israel
[b]Department of Mechanical Engineering, Northwestern University, 2145 Sheridan Road, Evanston, IL 6028, USA
[c]Department of Mechanical and Industrial Engineering, University of Illinois at Chicago, 842 West Taylor Street, Chicago, IL 60607-7022, USA

Received 12 July 2003; received in revised form 12 January 2004; accepted 15 January 2004

Abstract

In the electrospinning process, polymer nanofibers with submicron-scale diameters are formed when a droplet of a viscoelastic polymer solution is subjected to a high voltage electrostatic field. We report the experimental work on the electrospinning process in which the influence of different process parameters on the electric current and volume and surface charge density in the polymer jet was measured. Shear viscosity, surface tension, relaxation time, and the electric conductivity and permittivity were measured as well. For this purpose different solutions of polyethylene oxide (PEO), polyacrylic acid (PAA), polyvinyl alcohol (PVA), polyurethane (PU) and polycaprolactone (PCL) were prepared and underwent electrospinning. The governing parameters investigated were the applied voltage (V), the solution flow rate (Q), the polymer weight concentration (C), the molecular weight of the polymer (M), the nozzle-to-ground distance (H) and, in some solutions, the concentration of ethanol (C_{et}).

Keywords: Electrospinning; Governing parameters; Volume and surface charge density

1. Introduction

Electrospinning is a straightforward method to produce nanofibers from polymer solutions in a wide submicron range around 100 nm [1–4]. The interest in the behavior of thin liquid jets in electric fields dates back to the work of Rayleigh [5]. Taylor [6–9] produced useful experimental evidence on the conical shape of the protrusion from which a jet sometimes leaves the surface of a pendant liquid drop. A series of papers [10–17] in the electrospraying community have focused on the properties of liquid jets emitted from the Taylor cone. These papers demonstrate that with knowledge of the jet profile and the electric current it is possible to determine the volume charge density that enables an estimation of the electric field acting on the fluid boundary.

In electrospun jets emitted from Taylor cones, bending instability develops due to the mutually repulsive forces resulting from the electric charges of the jets [1,2]. Physical models [1,2,18–21] which examine the jet profile, the stability of the jet paths and the cone-like surfaces from which the jets emerge have been developed. In addition, it has been shown that capillary instability, resulting from surface tension, is typically prevented by the strong stabilizing influence of viscoelastic stresses [22] in the electrospinning of polymer solutions. With the recent revival of interest in electrostatic fiber spinning, there has been a number of innovative ideas that are being investigated, such as: electrically conductive nanofibers [23], nanofibrous membranes for the development of high performance batteries [24], piezoelectric nanofibrous devices [25], alignment of electrospun nanofibers [3, 26–28], electrospun nanofiber crossbars [29], nanotubes [30], nanofiber composites [31,32], electrospun mats for fine filtration [33], wound dressing [34], and fabrication of tubular products to serve as blood vessel prosthesis [26]. Development of useful applications requires a thorough knowledge of the parameters of the electrospinning process and their effect on the final product.

* Corresponding author. Address: Mechanical Engineering, Northwestern University, 2425 Sheridan Road, 60208 Evanston, United States. Tel./fax: +1-847-467-5298.
E-mail address: meeyal@tx.technion.ac.il (E. Zussman).

0032-3861/$ - see front matter © 2004 Elsevier Ltd. All rights reserved.
doi:10.1016/j.polymer.2004.01.024

In the present work we report the results of a systematic investigation of the effect of variation of the governing parameters on the electrospinning of PEO, PAA, PVA, PU and PCL solutions. The parameters investigated include: solution volumetric flow rate, polymer weight concentration and molecular weight, the applied voltage and the nozzle-to-ground distance. In addition, when using PEO solutions, we investigated the effect of the varying ethanol concentration in the solvent. The experimental setup and procedure are discussed in Section 2. This is followed in Section 3 by a presentation and discussion of the results obtained. A summary is provided in Section 4.

2. Experimental section

2.1. Materials

Polyethylene oxide (PEO, molecular weight $M = 6\times10^5$; 10^6; 4×10^6 g/mol), polyvinyl alcohol (PVA, $M = 10^4$ g/mol), polyacrylic acid (PAA, $M = 2.5\times10^5$; 4.5×10^5 g/mol), polyurethane (PU, Tecoflex) and polycaprolactone (PCL, $M = 8\times10^4$ g/mol) purchased from Aldrich were used to prepare solutions that were used as the working fluids. PEO, PVA and PAA were dissolved in an ethanol/water solvent at different concentrations. PU was dissolved in tetrahydrofuran (THF) and ethanol. PCL was dissolved in acetone and also in different blends of methylene chloride (MC, or dichloromethane) and dimethylformamide (DMF) at a temperature of 42 °C and cooled to room temperature before use. All chemicals and solvents were used as received. All solutions were stored at room temperature. All electrospinning experiments were carried out at room temperature in air.

2.2. Measurements and characterization

The electric conductivity and permittivity of the polymer solutions (σ and ε_r, respectively) were determined by measuring the complex impedance of a small cylindrical volume of fluid [35]. Surface tension (γ) measurements were conducted with a pulsating bubble surfactometer. Shear viscosities of the fluids were measured at different shear rates using a Couette viscometer (Brookfield DV-II + programmable viscometer). The relaxation times (θ) were determined using uniaxial elongational flow arising in self-thinning threads [36,37]. Relaxation times characterize viscoelastic properties of the electrospun solutions (cf. [1,2]). Relaxation times of PCL solutions could not be measured because of the high evaporation rates of solvents, acetone and methylene chloride (MC). Values of the above-mentioned parameters for the solutions used in this work are summarized in Table 1 for different polymer concentrations C (in wt%); the parameters for the solvents are shown in Table 2. Comparison of the surface tension of solutions of PEO ($M = 6\times10^5$ g/mol) in ethanol/water (40/60) to that of a pure blend of ethanol/water (40/60) suggests that the surface tension is mainly a function of the solvent in the solutions and tends to be less sensitive to variation in the polymer concentration.

Measurements of the shear viscosity at different shear rates for different solutions of PEO ($M = 6\times10^5$ g/mol) demonstrate a pronounced shear thinning, as shown in Fig. 1. The permittivity (ε_r) measurements for solvents and polymer solutions suggest that solvent properties dominate the solution values of ε_r. The conductivities of the solutions increase slightly with the addition of polymers. With the exception of PAA, the polymers used have very low conductivities; therefore it is assumed that σ is mostly a function of the ionic conductivity of slightly impure solvents.

2.3. Electrospinning setup

Experiments on electrospinning were performed with an apparatus basically similar to that used in the previous works [1–3]. A sketch of the experimental setup is depicted in Fig. 2. The electrospun nanofibers were collected on a large flat copper collector (400 mm × 400 mm). The collector was connected to ground through an Ohmic resistance. The potential drop over the resistance was measured and translated to electric current (I) using Ohm's law. The volume charge density (ρ) was calculated using Eq. (1)

$$\rho = \frac{I}{Q} \tag{1}$$

where I is the electric current and Q the volumetric flow rate. In our experiments the total resistor consisted of a 9 MΩ Ohmic resistor in series with an electronic low-pass filter (KemoVBF10) with an input impedance of 1 MΩ. Since all the measurements were done at low frequencies, the 1 MΩ input impedance was modeled as an Ohmic resistor. The 9 MΩ resistor served to reduce the total current through the electronic filter. The voltage drop over the

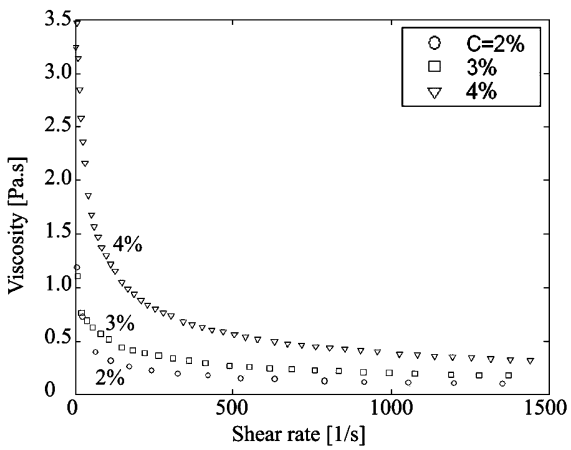

Fig. 1. Shear viscosity vs. shear rate. Plots for solutions of PEO ($M = 6\times10^5$ g/mol) in ethanol/water (40/60) at different weight concentrations.

Table 1
Characteristic properties of test fluids: molecular weight (M), polymer weight concentration (C), relative permittivity (ε_r), electric conductivity (σ), zero-shear viscosity (μ) and relaxation time (θ)

Polymer	M [g/mol])	Solvents	C [%]	ε_r	σ [mS/m]	μ [cP]	θ [ms]
PEO	6×10^5	Ethanol/water (40/60)	2	67.09	0.85	285	21
			3	61.44	1.38	1200	25
			4	66.57	1.15	3000	28
			6	57.63	1.67	43200	33
PEO	10^6	Ethanol/water (40/60)	2	66.71	0.81	1590	142
			3	67.97	1.28	9600	183
PEO	4×10^6	Ethanol/water (40/60)	1	66.12	1.102	4250	217
			2	70.07	1.45	90000	298
			3	65.07	0.88	335000	359
PEO	10^6	Water	2	81.96	9.43	570	–
	4×10^6		1	110.6	8.49	2600	128
PAA	2.5×10^5	Ethanol/water (40/60)	6	79.5	24.47	455	48.1
	4.5×10^5		5	74.14	17.95	255	22.75
PVA	10^4	Ethanol/water (50/50)	6	65.99	3.73	355	29.6
PU	Tecoflex	THF/ethanol (50/50)	6	16.75	0.093	25	–
			8	14.45	0.069	82	1.77
PCL	8×10^4	Acetone	8	25.2	0.142	107	–
			10	25.38	0.141	165	–
			14	24.8	0.12	400	–
PCL	8×10^4	MC/DMF (75/25)	10	18.55	0.191	670	–
		MC/DMF (40/60)	10	24.49	0.36	950	–

1 MΩ impedance was measured in order to compute the electric current. The electronic filter was used to filter out frequencies above 10 Hz (mainly a 50 Hz signal of the power network). The output of the digital filter was sampled with a PC using a DAQ device (National Instruments PCI 6024E).

The initial volume charge density is often used as a given parameter in the models of electrospinning, cf. [1,2]. The initial volume charge density can be estimated when the volumetric flow rate of the solution is controlled. The volume charge density can be used to calculate the surface charge density. Indeed, almost all the free charges are located at the jet surface after it has been issued from the Taylor cone [38]. However, the jet evaporates, stretches, bends and sometimes branches under the action of the electric field. As a result, the surface charge density varies along the jet. Therefore the results presented in terms of the surface charge density are inevitably geometry- and case-dependent to a much higher extent than those for the initial volume charge density. That is the reason that the present work mostly uses the initial volume charge density carried by the electrospun jet.

However, for comparison, the surface charge density (q) for one solution of PCL was determined at different applied voltages (12–20 kV) and volumetric flow rates (200–600 μl/min). The surface charge density was determined

Table 2
Characteristic properties of solvents: relative permittivity (ε_r), electric conductivity (σ), viscosity (η) and surface tension (γ)

Solvents	ε_r	σ [mS/m]	η [cP]	γ [mN/m]
Distilled water	88.75	0.447	1.12	72
Ethanol (95%)	24.55[a]	0.0624	1.1[a]	22.3[a]
Acetone	20.7[a]	0.0202	0.36[a]	23.3[a]
Ethanol/water (40/60)	69.47	0.150	2.49	30[b]
MC/DMF (40/60)	29.82	0.505	0.93	31.6
MC/DMF (75/25)	21.3	0.273	0.73	28.9
THF/ethanol (50/50)	15.79	0.037	0.89	23.7

[a] http://www.bandj.com/Home.html.
[b] Wohlfarth, Ch., Wohlfarth, B., 1997. In: Lechner, M.D. (Ed.), Surface Tension of Pure Liquids and Binary Liquid Mixtures. Springer, New York.

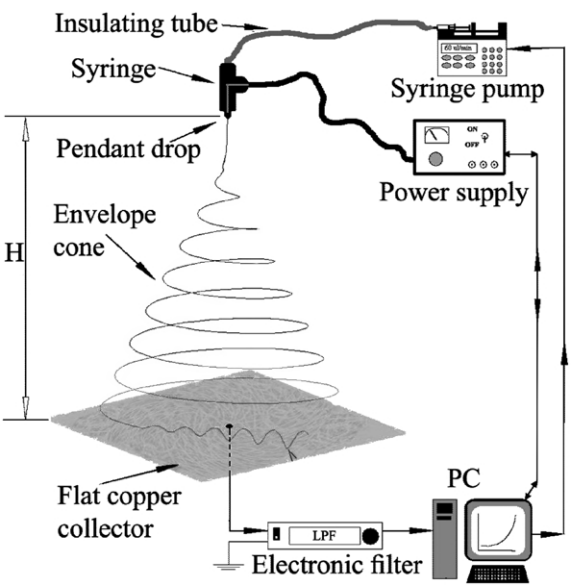

Fig. 2. Sketch of the experimental setup for measuring the electric current in electrospun jets.

only for a single cross-section of the jet near the Taylor cone (2 mm from the orifice of the polymer bath). It was assumed that variation of the volume charge density due to evaporation above this cross-section was negligible. Measurements of the jet diameter near the Taylor cone could not be done accurately enough for the applied voltages and volumetric flow rates, since the jet diameter, d decreases very rapidly in this area. The latter introduced an inaccuracy in the measurement of the jet diameter and contributed to the inaccuracies in the values of the surface charge densities obtained via this procedure. In the case when the initial volume charge density was to be recast into the surface charge density, the following procedure was used. The jet diameter was measured with the aid of high speed photography. Diameters between 20 and 60 μm were recorded just below the tip of the cone where the jet is initiated (2 mm from the orifice). This is in agreement with the work of Doshi et al. [39]. The surface charge density was calculated as per

$$q = \frac{\rho d}{4} 10^{-7} \tag{2}$$

where d [μm] is the measured diameter of the jet close to the tip of the Taylor cone, q [C/cm^2] the surface charge density calculated at the point of measurement, and ρ [C/l] as found from Eq. (1).

The area around the Taylor cone tip was photographed with a high speed digital imaging system (Redlake Motionscope® PCI system). The camera was equipped with an Edmund Scientific zoom lens (VZM™ 450). Images were captured at 50 fps and at a shutter speed of 1.3 ms.

A high voltage power supply (Gamma High Voltage Research, XRM30P) was used to control the applied voltage. As in the work of Shin et al. [40], no effort was made to produce a uniform electric field between the electrode attached to the solution in the syringe and the grounded collector. In our setup, the electric field strength shows a maximum value at the droplet/Taylor cone tip and is highly non-uniform. The maximum field strength in this non-uniform field is much higher than the value in the corresponding parallel capacitor field. The results are given in terms of the applied voltage rather than the electric field strength, since the electric field could only be determined through detailed numerical calculations, whereas the applied voltage was fixed on the electrode with the high voltage power supply. During the experiments special care was taken to avoid any ionization current via the air gap (or to minimize it as much as possible) when no electrospun jet was present.

In the current experiment, the solution supply rate was adjusted with a digitally controlled syringe pump (Harvard Apparatus, PHD 2000), which was electrically insulated from the syringe that contained the test fluid by a hydraulic connection denoted as the 'insulating tube' in Fig. 2. The solution flow rate was controlled in the sense that the solution was prevented from being drawn out of the nozzle faster than it was supplied, since in such a situation a vacuum would be formed in the system. Nonetheless, at low supply rates the possibility existed that the electrospinning process could be stopped momentarily. In our experiments, electrical currents were measured for values of the applied voltage and solution supply rate where no interruption in the electrospinning process occurred. However, oscillations did appear (depending on the applied voltage) in the solution flow rate. While the oscillations could be seen by observing the Taylor cone, their effect could not be detected during the current measurement, since only average values of the electric current were measured during the experiments. Competition between supply of the solution by the syringe pump and its withdrawal caused by the electric field leads to the change in shape and volume of the region where the jet leaves the tip, which is obviously the reason for the oscillations. Future theoretical work could elucidate the nature and detailed characteristics of this interaction. For every supply rate chosen during the experiments, there existed a corresponding electric field strength (adjusted by the applied voltage), where the oscillations in the flow rate disappeared. In the present work the shape and volume of the region where the jet leaves the tip were fixed and constant for all experiments. The average solution flow rate between the nozzle and the ground collector was assumed to be equal to the solution supply rate (controlled by the syringe pump).

Electrospinning typically results in bending instability of the jet beginning at some distance from the droplet tip [1,2]. For PEO solutions, however, bending instability was not always observed. At higher electric field strengths and higher flow rates the bending instability disappeared, resulting in a straight jet over the whole electrode-to-ground distance. Additionally, the bending instability appeared more readily in PEO solutions with lower molecular weights, where the stabilizing effect of viscoelastic stresses is reduced. According to our measurements, the disappearance of the bending instability under certain conditions did not have a noticeable effect on the volume charge density carried by the jet. For the purpose of this discussion, all the solutions of PEO contained 40% ethanol and 60% water, unless otherwise indicated.

3. Results and discussion

The electric current and the volume charge density display the same behavior with respect to all the investigated governing parameters except the solution flow rate.

3.1. Applied voltage (V)

Experimental data for the current/voltage measurements of PEO, PAA, PVA, PU and PCL solutions at fixed values of the volumetric flow rate are shown in Fig. 3. The

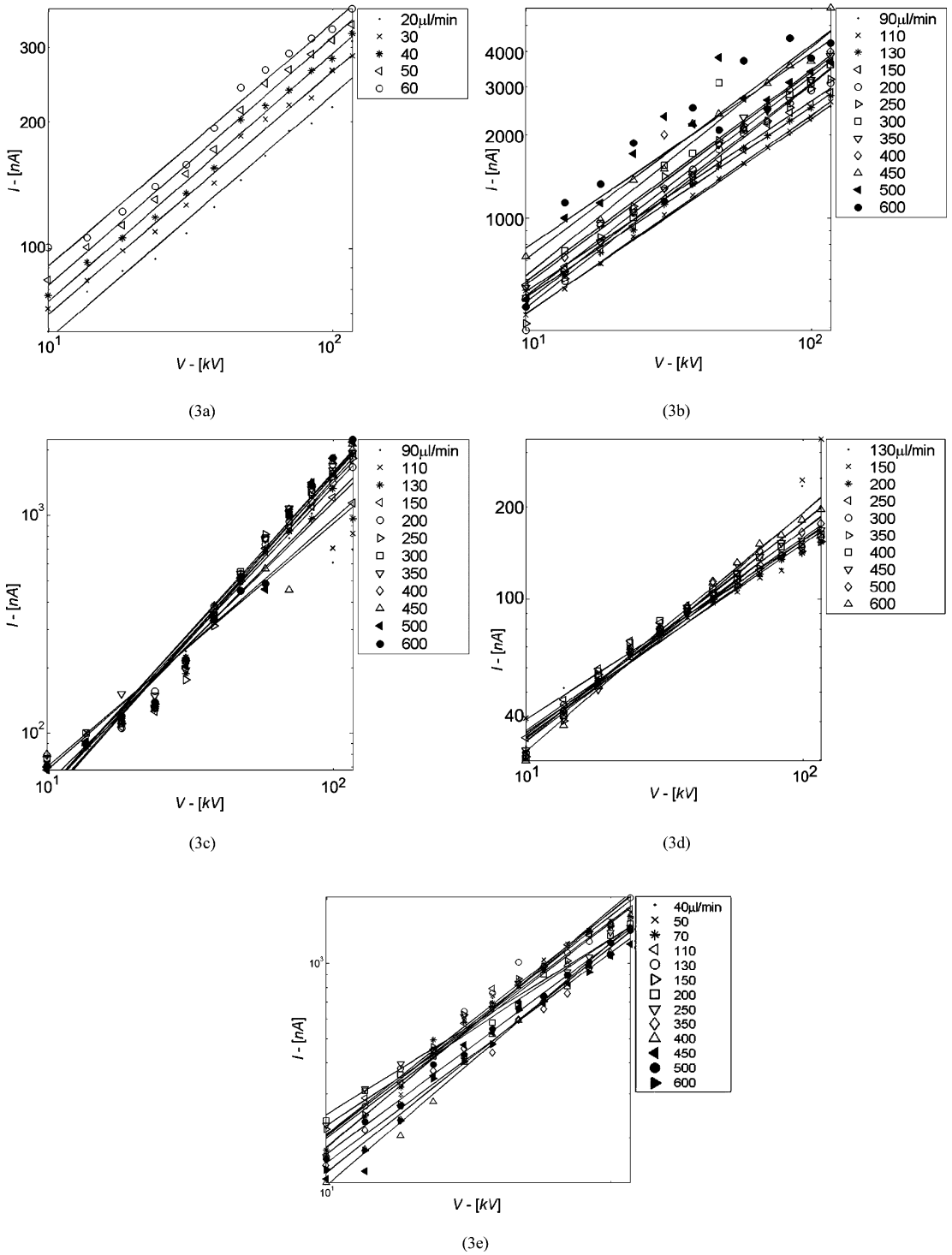

Fig. 3. The electric current (I) vs. the applied voltage (V) for different polymer solutions at different flow rates. (a) PEO, $M = 6 \times 10^5$ g/mol, $C = 2\%$, ethanol/water = 40/60; (b) PAA, $M = 2.5 \times 10^5$ g/mol, $C = 6\%$, ethanol/water = 40/60; (c) PVA, $M = 1 \times 10^4$ g/mol, $C = 6\%$, ethanol/water = 50/50; (d) PU, Tecoflex, $C = 6\%$, THF/ethanol = 50/50; (e) PCL, $M = 8 \times 10^4$ g/mol, $C = 10\%$, MC/DMF = 40/60.

corresponding data for the volume charge density vs. the applied voltage are shown in Fig. 4. The values of the electric current for PEO solutions are of the same order as the values obtained by Shin et al. [40]. For all the solutions tested, both I and ρ as functions of V approach a power law relationship as the applied voltage increases. Eqs. (3) describe these relationships

$$I(V) = k_{IV} V^{p_V} \tag{3a}$$

$$\rho(V) = k_{\rho V} V^{p_V} \tag{3b}$$

The value of the exponent p_V changes somewhat from

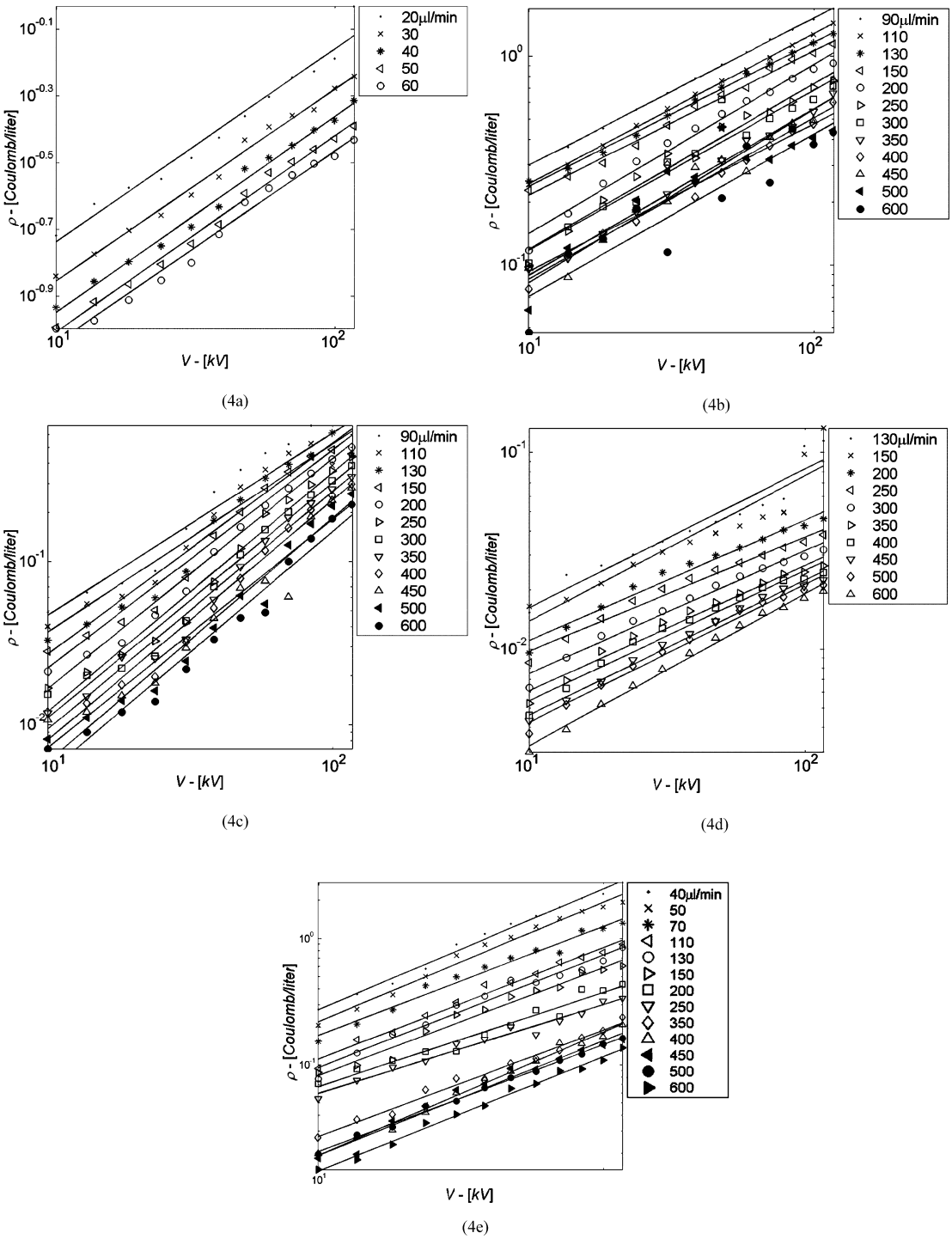

Fig. 4. The volume charge density (ρ) vs. the applied voltage (V) for different polymer solutions at different flow rates. (a) PEO, $M = 6 \times 10^5$ g/mol, $C = 2\%$, ethanol/water = 40/60; (b) PAA, $M = 2.5 \times 10^5$ g/mol, $C = 6\%$, ethanol/water = 40/60; (c) PVA, $M = 1 \times 10^4$ g/mol, $C = 6\%$, ethanol/water = 50/50; (d) PU, Tecoflex, $C = 6\%$, THF/ethanol = 50/50; (e) PCL, $M = 8 \times 10^4$ g/mol, $C = 10\%$, MC/DMF = 40/60.

solution to solution. For solutions of PEO in ethanol and water, it is close to 3. The PU solutions employed in the present work yielded the value $p_V = 2.17$. Demir et al. [41], who studied the behavior of PU solutions, also reported a power law behavior for I as a function of V with $p_V = 2.7$ The values of k_{IV} and $k_{\rho V}$ increase with increasing volumetric flow rates (cf. Figs. 3 and 4). The mean values of p_V for all the solutions studied are summarized in Table 3.

Demir et al. [41] working with PU solutions reported a power law relationship between the solution flow rate (Q) and the applied voltage (V) with an exponent value of three in the experiments where Q was not controlled. In contrast

Table 3
Summary of the exponents in the approximations of Eqs. (3) to (13)

Polymer	M [g/mol]	C [%]	p_V	p_{qV}	$p_{\rho Q}$	p_{qQ}	p_{IQ}	p_C	p_M	h [cm]	p_{Cet}
PEO	6×10^5	2, 3, 4	2.614	–	−0.754	–	0.246	0.579	–	–	–
	1×10^6	1, 2, 3, 5	3.267	–	−0.776	–	0.224	0.69	–	–	–
	4×10^6	0.1, 1, 2, 3	2.948	–	−0.814	–	0.186	0.517	–	–	–
	4×10^6	1	–	–	–	–	–	–	–	–	−0.11
	6×10^5	2	–	–	–	–	–	–	–	45.5	–
	1×10^6	2	–	–	–	–	–	–	–	35.37	–
	4×10^6	2	–	–	–	–	–	–	–	30.78	–
	6×10^5, 10^6, 4×10^6	2	–	–	–	–	–	–	0.9	–	–
	6×10^5, 10^6, 4×10^6	3	–	–	–	–	–	–	0.55	–	–
PVA	10^4	6	4.565	–	−0.743	–	0.257	–	–	–	–
PAA	2.5×10^5	6	2.505	–	−0.738	–	0.262	–	–	–	–
	4.5×10^5	5	3.729	–	−1.023	–	−0.023	–	–	–	–
PU	Tecoflex	6, 8	2.166	–	−0.845	–	0.155	–	–	–	–
PCL MC/DMF(75/25)	8×10^4	10	3.218	–	−0.967	–	0.033	–	–	–	–
PCL MC/DMF(40/60)	8×10^4	10	2.891	4.0	−1.114	−0.83	−0.114	–	–	–	–
PCL (acetone)	8×10^4	8, 10, 14	3.11	–	−2.04	–	−1.04	0.19	–	–	–

to this, Fong et al. [42] working with PEO solutions reported a linear relationship. Baumgarten [43] showed that the diameter of the jet initially decreases as the field strength increases and then begins to increase as the field strength still increases. This, in fact, means an increase in volumetric flow rate as the applied voltage increases beyond a certain level. The phenomenon is related to the fact that increasing the field increases the electrostatic stresses, which in turn, draw more material out of the syringe. Doshi [44] plotted the jet diameter at different positions along the jet. He showed that at the capillary exit, there was a threefold increase in the diameter resulting from less than a twofold increase in the applied voltage in the experiments where Q was not controlled.

Fig. 5 shows the plots of the surface charge density (q) vs. the applied voltage for the PCL with $M = 8\times10^4$, $C =$ 10%, MC/DMF = 40/60. The solid lines represent the fitted data according to the following equation

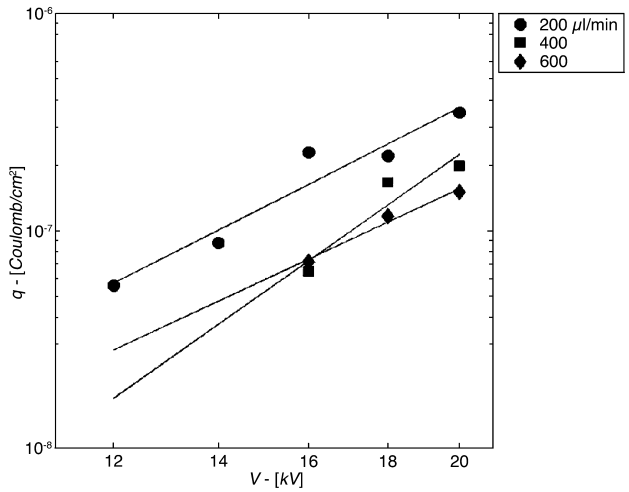

Fig. 5. Surface charge density (q) vs. the applied voltage (V) for the PCL solution with $M = 8\times10^4$ g/mol, $C = 10\%$, MC/DMF = 40/60.

$$q = k_{qV}V^{p_{qV}} \tag{4}$$

The general behavior of the surface charge density is similar to that of the volume charge density. The average value of p_{qV} was 4.0. This value is higher than that of $p_{\rho V}$, which was 2.891 for the same solution. The factor k_{qV} increased with increasing volumetric flow rate.

3.2. Solution flow rate (Q)

Figs. 6 and 7 show characteristic plots of I and ρ as functions of the volumetric flow rate Q, respectively, for several fixed values of the applied voltage for the solutions of PEO, PAA, PVA, PU and PCL. Both I and ρ, as functions of Q, exhibit a power law behavior according to Eqs. (5) and (6)

$$I(Q) = k_{IQ}Q^{p_{IQ}} \tag{5}$$

$$\rho(Q) = k_{\rho Q}Q^{p_{\rho Q}} \tag{6}$$

The mean values of p_{IQ} and $p_{\rho Q}$ for different solutions are given in Table 3. The value of the exponent p_{IQ} is dependent upon the solution. In most cases I increases, while ρ decreases as a function of flow rate. The value of the exponent $p_{\rho Q}$ for all polymer solutions is negative. According to Eq. (1), $p_{\rho Q} = p_{IQ} - 1$ which is also seen in Table 3. Ref. [17] reports that in the case of electrospraying of 1-octanol seeded with sulfuric acid there also exists a power law relationship between I and Q with an exponent value of 0.5. The values of k_{IQ} and $k_{\rho Q}$ increase with increasing the applied voltage (cf. Figs. 6 and 7).

Fig. 8 depicts the plots of the surface charge density vs. volumetric flow rate for the same solution as that in Fig. 5. The solid lines are fitted according to the following equation

$$q = k_{qQ}Q^{p_{qQ}} \tag{7}$$

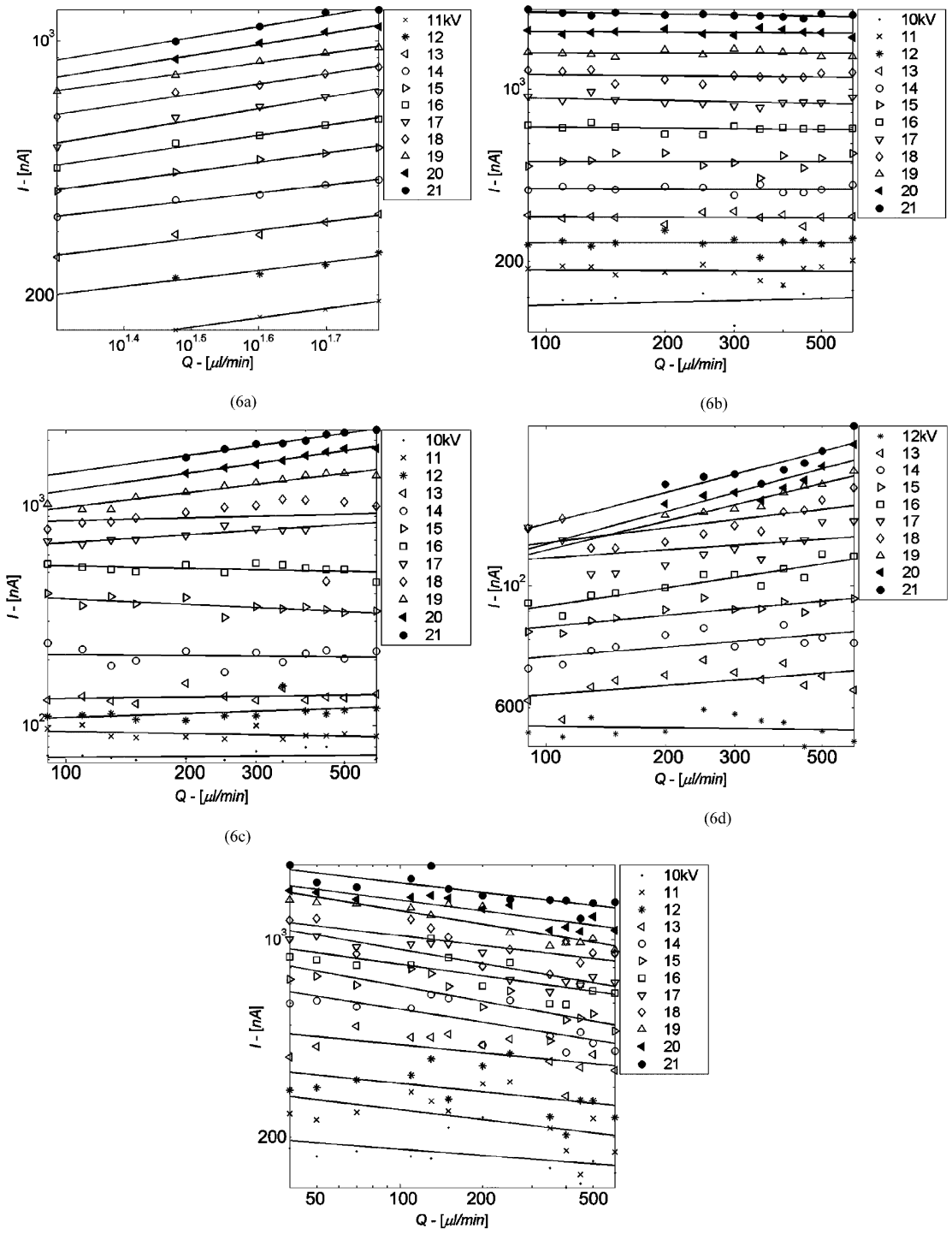

Fig. 6. The electric current vs. volumetric flow rate. (a) PEO, $M = 6 \times 10^5$ g/mol, $C = 3\%$, ethanol/water = 40/60; (b) PAA, $M = 4.5 \times 10^5$ g/mol, $C = 5\%$, ethanol/water = 40/60; (c) PVA, $M = 1 \times 10^4$ g/mol, $C = 6\%$, ethanol/water = 50/50; (d) PU, Tecoflex, $C = 6\%$, THF/ethanol = 50/50; (e) PCL, $M = 8 \times 10^4$ g/mol, $C = 10\%$, MC/DMF = 40/60.

The average value of p_{qQ} was -0.83. As in the case of the applied voltage, the value of p_{qQ} is slightly higher than $p_{\rho Q}$.

The reason for the decrease of ρ as a function of Q can be explained by analyzing the charge flow in the polymer bath. Fig. 9 shows a schematic drawing of the polymer bath used during the current measurements. Higher flow rates can lead to a faster removal of the ions at the orifice side of the polymer bath. However, this effect seems to be rather insignificant. Indeed, below we show that the rate of replenishment of the ion concentration at the orifice side is

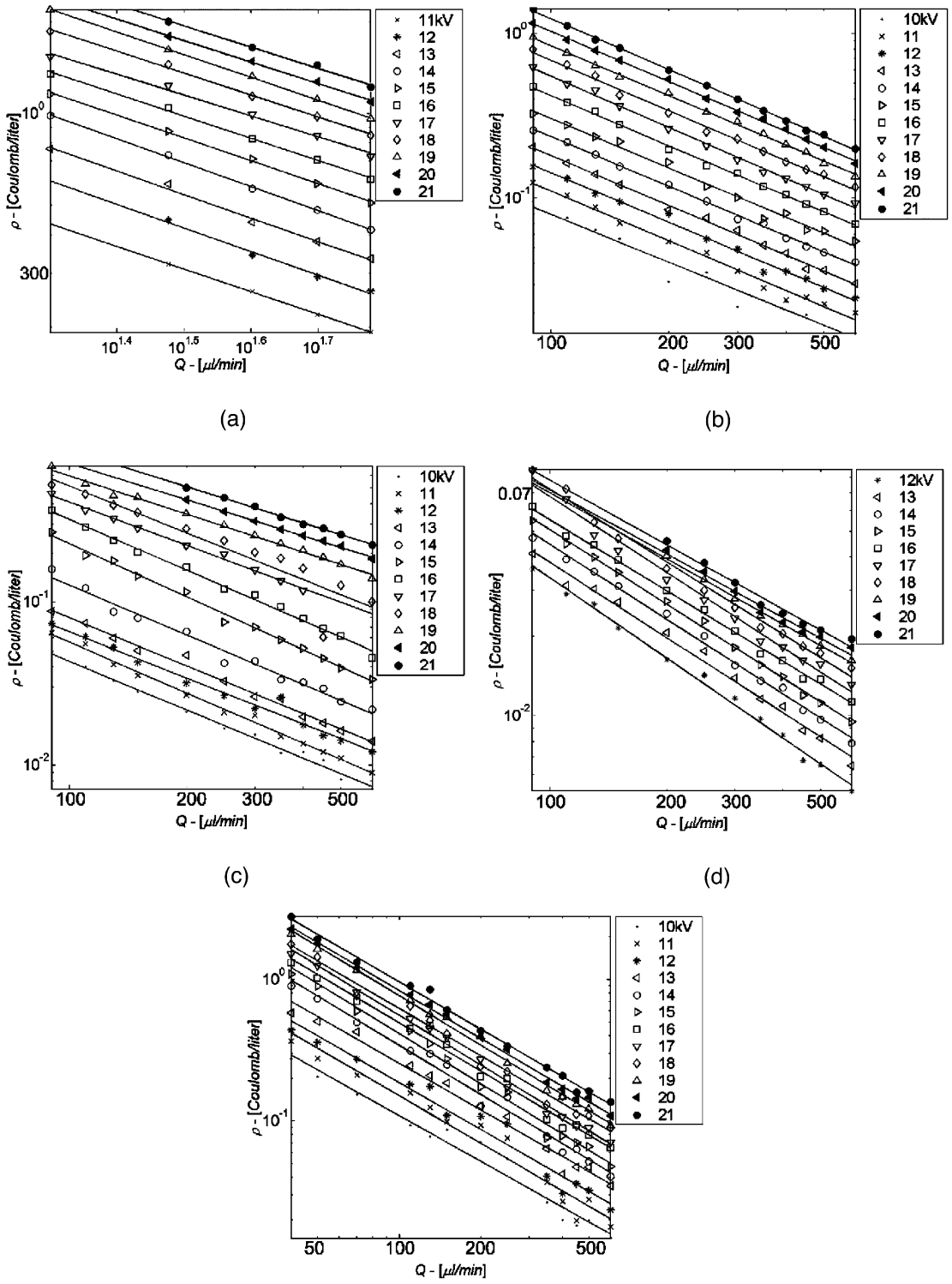

Fig. 7. The volume charge density vs. volumetric flow rate. (a) PEO, $M = 6 \times 10^5$ g/mol, $C = 3\%$, ethanol/water = 40/60; (b) PAA, $M = 4.5 \times 10^5$ g/mol, $C = 5\%$, ethanol/water = 40/60; (c) PVA, $M = 1 \times 10^4$ g/mol, $C = 6\%$, ethanol/water = 50/50; (d) PU, Tecoflex, $C = 6\%$, THF/ethanol = 50/50; (e) PCL, $M = 8 \times 10^4$ g/mol, $C = 10\%$, MC/DMF = 40/60.

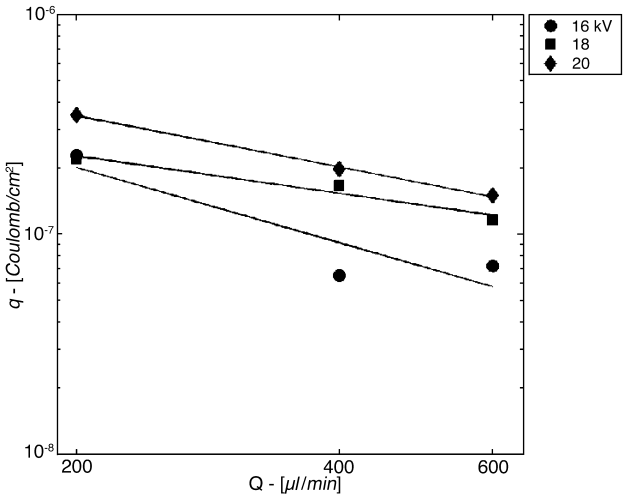

Fig. 8. Surface charge density (q) vs. volumetric flow rate (Q) for the PCL solution with $M = 8 \times 10^4$ g/mol, $C = 10\%$, MC/DMF = 40/60.

mostly determined by the drift velocity of the ions as given by Eq. (8) (see [45,46])

$$\mathbf{v}_\mathrm{d} = \frac{e_0 z_i}{6\pi a \eta}\mathbf{E}, \tag{8}$$

where $\mathbf{v}_\mathrm{d}$ is the drift velocity, e_0 is the absolute value of the charge of an electron, z_i is the valence of the charge carriers (mainly impurities in the solutions in our case), η the solvent viscosity, a the mean radius of the charge carriers (ions) and $\mathbf{E}$ the effective electric field inside the polymer bath. $|\mathbf{E}|$ (inside the polymer bath) was obtained experimentally by measuring the voltage difference between the electrode and a point on the nozzle where the polymer exits. $|\mathbf{E}|$ was also calculated for the current setup using the finite element method. The measured and calculated values of $|\mathbf{E}|$ were of the order of $1{\cdot}\mathrm{g}^{1/2}(\mathrm{cm}^{1/2}{\cdot}\mathrm{s})$ (which is 300 V/cm). Using the following values: $e_0 = 4.8 \times 10^{-10}$ ($\mathrm{g}^{1/2}$ $\mathrm{cm}^{3/2}$)/s (which is 1.6×10^{-19} C); $z_i = +1$; $\eta = 10^{-2} - 10^{1}$ g/(cm s) (which is 1–1000 cP) and $a = 10^{-8}$cm, $|\mathbf{v}_\mathrm{d}|$ is estimated to be of the order of $1\text{–}10^{-3}$cm/s. This value allows for a time delay of a few seconds before newly created ions arrive at the orifice of the polymer bath. On the other hand, the fluid velocity in the syringe during electrospinning was estimated (from images taken with a high speed camera) to be of the order of 10^{-4} cm/s. This is much smaller than the drift velocity of the ions. Therefore, the rate of replenishment of the ion concentration appears to be virtually independent of Q. On the other hand, the rate of withdrawal of the opposite charges by the electrode is obviously dependent on the residence time of ions in contact with the needle (Fig. 9). At higher flow rates, fewer (negative) ions are withdrawn into the needle. Therefore, the fluid carries a lower (positive) excessive charge at the time it arrives at the syringe orifice. This conclusion holds even though some ions end up at the inner wall of the syringe. As a result, the volume charge in the jet should decrease at higher Q.

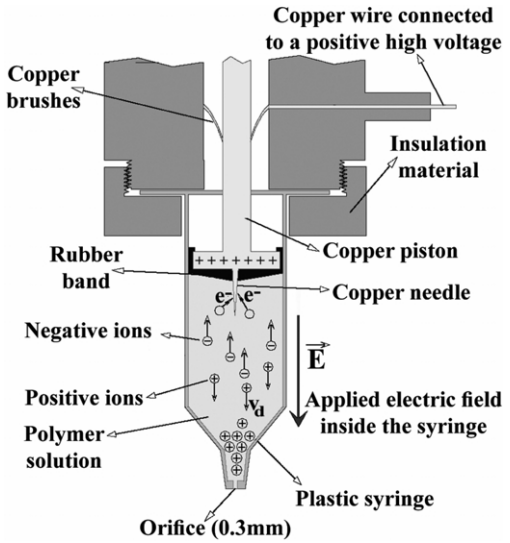

Fig. 9. Sketch of the syringe bath used in the measurement of the electric current.

The dependence of the volume charge density and the current on the applied voltage for a single fixed volumetric flow rate is depicted in Fig. 10. It should be noted that the volume charge density for the PCL and PU solutions is much lower than for the PEO solutions. In Ref. [47] it is suggested that the appearance of the garland structure in the electrospinning of some PCL solutions results from a low volume charge density in the electrospun solution, which is supported by the present data. Also, the fact that the volume charge density decreases as a function of the volumetric flow rate supports this assumption. In the case of the PCL and PU solutions, when the flow rates were drastically increased, the low volume charge density decreased even more, as a result. In these cases, the reduction of the electric volume charge density allowed for the merging of different sections of the fiber in flight, thus facilitating the formation of garlands as in Ref. [47]. This never happens with highly charged PEO jets.

3.3. Polymer concentration (C)

The electric current (I) as a function of polymer weight concentration (C) is depicted in Fig. 11 for PEO. Eqs. (9) approximate the relationships obtained as

$$I(C) = k_{IC} C^{p_C}. \tag{9a}$$

$$\rho(C) = k_{\rho C} C^{p_C}. \tag{9b}$$

For PEO $p_C = 0.5 - 0.6$. The values of k_{IC} and $k_{\rho C}$ increased with the applied voltage. The mean values of p_C are given in Table 3 for different solutions.

3.4. Molecular weight (M)

With respect to molecular weight, the current and volume charge density also behave according to a power

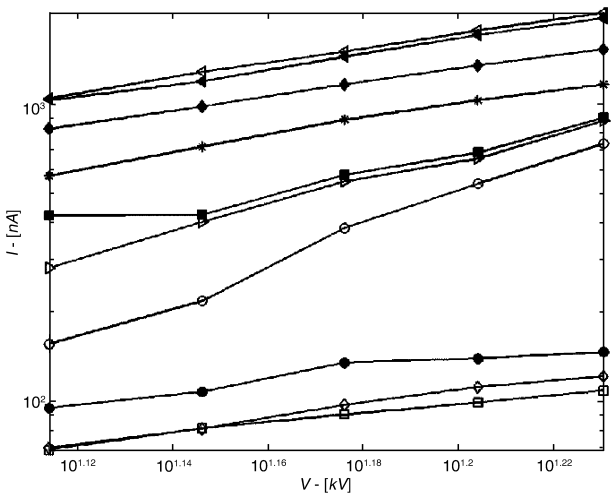

Fig. 10. (a) The electric current I as a function of V for different polymer solutions. (b) Plot of ρ as a function of V. The volumetric flow rate (Q) in both (a) and (b) was 200 μl/min. The data in the graph are depicted using the following symbols: (∗) PEO ($M = 4 \times 10^6$ g/mol), $C = 1\%$, ethanol/water = 40/60; (○) PVA ($M = 10^4$ g/mol), $C = 6\%$, ethanol/water = 50/50; (□) PU (Tecoflex), $C = 6\%$, THF/ethanol = 50/50; (◇) PU (Tecoflex), $C = 8\%$, THF/ethanol = 50/50; (◁) PAA ($M = 2.5 \times 10^5$ g/mol), $C = 6\%$, ethanol/water = 40/60; (▷) PAA ($M = 4.5 \times 10^5$ g/mol), C = 5%, ethanol/water = 40/60; (●) PCL ($M = 8 \times 10^4$ g/mol), $C = 10\%$, MC/DMF = 75/25; (■)PCL ($M = 8 \times 10^4$ g/mol), $C = 10\%$, MC/DMF = 40/60; (◆) PEO ($M = 10^6$ g/mol), $C = 2\%$, $C_{et} = 0\%$; (◀) PEO ($M = 4 \times 10^6$ g/mol), $C = 1\%$, $C_{et} = 0\%$.

law [Eqs. (10)] as depicted in Fig. 12

$$I(M) = k_{IM} M^{p_M} \tag{10a}$$

$$\rho(M) = k_{\rho M} M^{p_M} \tag{10b}$$

The values of k_{IM} and $k_{\rho M}$ increased with the applied voltage. The mean values of p_M are given in Table 3.

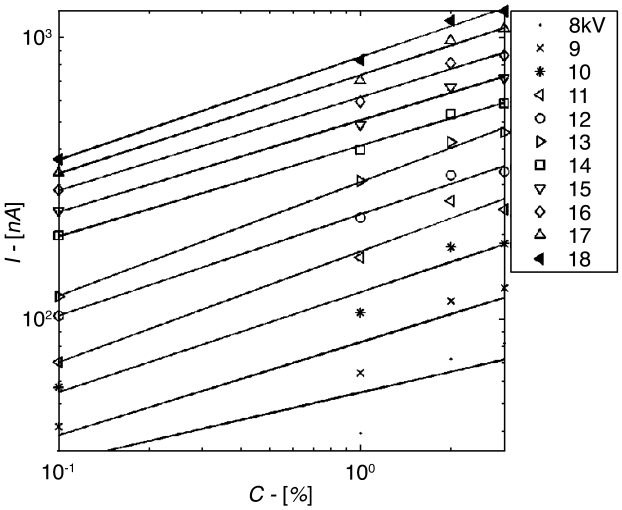

Fig. 11. The electric current vs. polymer weight concentration for PEO, $M = 4 \times 10^6$ g/mol at $Q = 20$ μl/min.

3.5. Nozzle-to-ground distance (H)

The following exponential expressions describe the dependence of I and ρ on the nozzle-to-ground distance (H)

$$I(H) = k_{IH} e^{-H/h}, \tag{11a}$$

$$\rho(H) = k_{\rho H} e^{-H/h}, \tag{11b}$$

which approximates the results shown in Fig. 13. In Eqs. (11) h is a constant with the same dimension as H. The parameter h as a function of M is shown in Fig. 14. The following power law equation was fitted to the three points shown in Fig. 14:

$$h(M) = k_{hM} M^{p_{hM}}, \tag{12}$$

where $k_{hM} = 43.66$ and $p_{hM} = -0.496$.

The fact that the volume charge density decreases as H

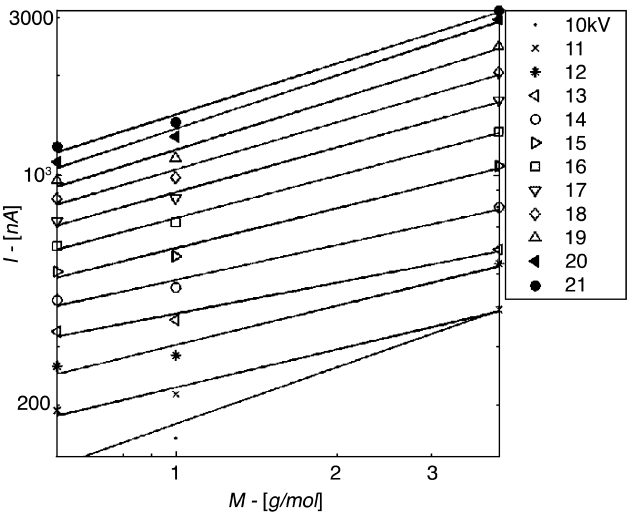

Fig. 12. The electric current vs. polymer molecular weight for PEO, $C = 3\%$ at $Q = 60$ μl/min.

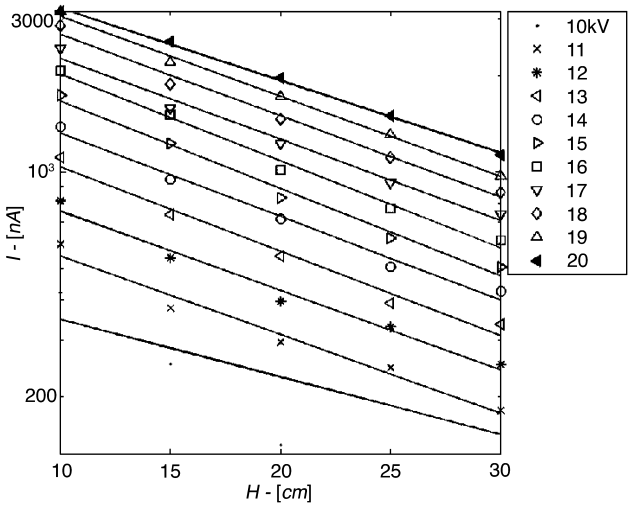

Fig. 13. The electric current vs. nozzle-to-ground distance for PEO, $M = 4 \times 10^6$ g/mol, $C = 1\%$ at $Q = 30$ μl/min.

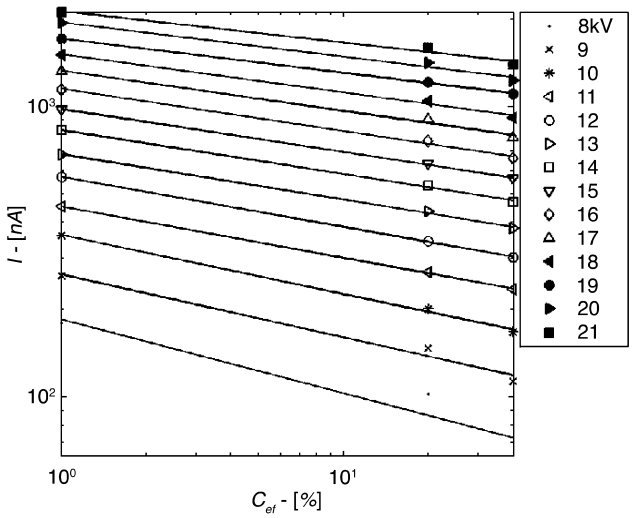

Fig. 15. The electric current as a function of the concentration of ethanol in PEO solutions with $M = 4 \times 10^6$ g/mol, $C = 1\%$ at $Q = 30$ μl/min.

increases is a result of the decrease in the electric field strength as H increases at a constant applied voltage.

3.6. Concentration of ethanol in solution (C_{et})

PEO solutions in pure water followed the power law relationships of Eqs. (3) more accurately than PEO solutions that contain ethanol. Fong et al. [42] reported that with the addition of ethanol to aqueous solutions of PEO, the net volume charge density carried by the jet decreased. The electric current I as a function of C_{et} is plotted in Fig. 15 and is approximated by Eq. (13):

$$I(C_{et}) = k_{IC_{et}} C_{et}^{p_{Cet}}, \tag{13a}$$

$$\rho(C_{et}) = k_{\rho C_{et}} C_{et}^{p_{Cet}}, \tag{13b}$$

where the average value of p_{Cet} is -0.11. It is emphasized that as the amount of ethanol in the solution increases, the amount of water decreases in order to keep the weight concentration of polymer constant. Solutions were electrified after preparation, and those with a higher amount of ethanol displayed a lower volume charge density. This can be attributed to the fact that the impurities responsible for the charge carriers are mostly brought by water.

The results of this subsection show that the main positive effect of ethanol in a solution undergoing electrospinning is not created by any alteration of the charge, but arises from an increase in the solution evaporation rate which has been shown to facilitate nanofiber solidification.

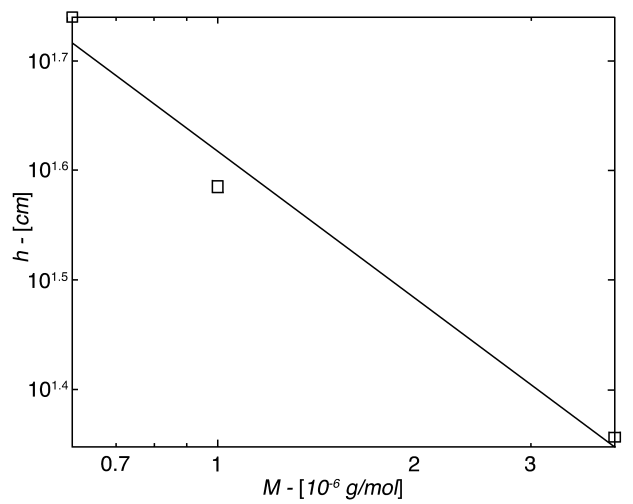

Fig. 14. Parameter h as a function of the molecular weight (M) for solutions of PEO ($C = 2\%$ and $Q = 30$ μl/min). The solid line corresponds to: $h(M) = 43.66 \times M^{-0.496}$; the standard deviation is 5.33.

3.7. Parameter combination

The mean experimental values of the exponents in Eqs. (3) through (13) are summarized in Table 3. When combining the approximations of Eqs. (3) through (13), the volume charge density can be described by the following cumulative equation:

$$\rho = k_{exp} V^{p_V} Q^{p_{\rho Q}} C^{p_C} M^{p_M} \mathbf{e}^{-H/h} C_{et}^{p_{Cet}}, \tag{14}$$

where k_{exp} may depend on such parameters as the intrinsic solution properties, temperature and humidity. Eq. (14) was used to calculate the volume charge density for PEO solutions using the following average values from Table 3:

$$p_V = 3;\ p_{\rho Q} = -0.8;\ p_C = 0.75;\ p_M = 0.5;\ p_{Cet} = -0.11. \tag{15}$$

The value of h was found from Eq. (12). The factor k_{exp} was estimated using the measured values of ρ and appeared to be about 0.0128 with the standard deviation of 0.00556, as shown in Fig. 16. Not all the experiments were carried out at the same time and with exactly the same solution samples. The jumps in the value of k_{exp} could result from variation in

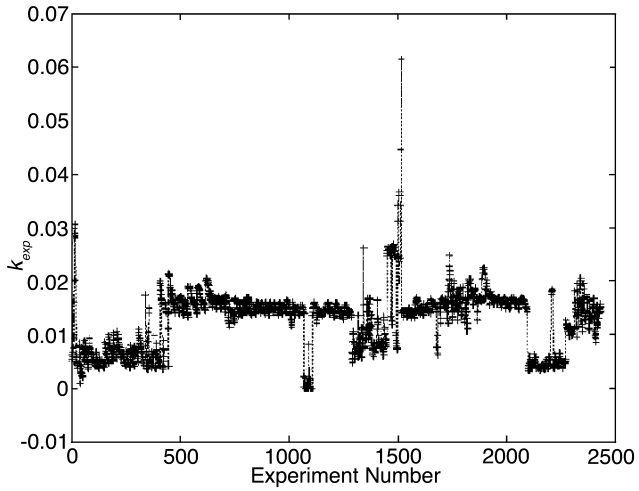

Fig. 16. The factor k_{exp} for a number of experiments. The mean value is 0.0128 and the standard deviation is 0.00556.

temperature and humidity and also from the variation in the physical parameters between fresh and older solutions.

4. Summary

The relevant physical parameters were measured for a number of polymer solutions (PEO, PAA, PVA, PU and PCL in different solvents) used in the electrospinning of polymer nanofibers. The experiments were undertaken to determine variation of the electric current (I) and volume charge density (ρ) in response to changes in the governing parameters of the process. In the case of one PCL solution the surface charge density q was determined as well. The governing parameters investigated include the applied voltage (V), the solution flow rate (Q), polymer concentration (C), molecular weight (M), nozzle-to-ground distance (H), and the ethanol concentration in the solvents (C_{et}) for PEO solutions. The values of the electric permittivity, conductivity, zero-shear viscosity, surface tension and relaxation time were also measured.

We found that the volume charge density follows power law dependences on V, Q, C, M, and C_{et} and depends exponentially on H. These relationships are summarized in Eqs. (3) through (13). In addition, the volume charge density (ρ) decreases with increasing flow rate (Q) for all the solutions tested. The dependences of the surface charge density q on V and Q are similar to those for ρ. In contrast to this, the electric current (I) in the jet increases with Q for some solutions (PEO, PVA, PAA $M = 2.5 \times 10^5$ and PU), but decreases for the other solutions (PCL). For the solution of PAA of $M = 4.5 \times 10^5$ it appears as if the electric current is not affected at all by the volumetric flow rate. Decrease in ρ at higher values of the volumetric flow rate Q is attributed to a low residence time of the solution near the electrode. The fact that the volume charge density decreases exponentially as H increases is explained by the decrease in the electric field strength as H increases at a constant applied voltage. The addition of ethanol to an aqueous PEO solution decreases the volume charge density when all the other parameters are kept constant. This shows that the main positive effect of ethanol in a mixture undergoing electrospinning is not related to the volume charge density, but rather to a higher evaporation rate, which facilitates nanofiber solidification.

References

[1] Reneker DH, Yarin AL, Fong H, Koombhongse S. Bending instability of electrically charged liquid jets of polymer solutions in electrospinning. J Appl Phys 2000;87:4531–47.
[2] Yarin AL, Koombhongse S, Reneker DH. On bending instability in electrospinning of nanofibers. J Appl Phys 2001;89:3018–26.
[3] Theron A, Zussman E, Yarin AL. Electrostatic field-assisted alignment of electrospun fibers. Nanotechnology 2001;12:384–90.
[4] Bognitzki M, Czando W, Frese T, Schaper A, Hellwig M, Steinhart M, Greiner A, Wendorff JH. Nanostructured fibers via electrospinning. Adv Mater 2001;13:70–2.
[5] Strutt JW. On the equilibrium of liquid conducting masses charged with electricity, London, Edinburgh, Dublin. Philos. Mag. 1882;14: 184–6.
[6] Taylor GI. Disintegration of water drops in an electric field. Proc R. Soc. London, Ser. A 1964;280:383.
[7] Taylor GI. Stability of a horizontal liquid interface. J Fluid Mech 1965;22:1.
[8] Taylor GI. The force exerted by an electric field on a long cylindrical conductor. Proc. R. Soc. London, Ser. A 1966;291:145.
[9] Taylor GI. Electrically driven jets. Proc R. Soc. London, Ser. A 1969; 313:453.
[10] Melcher JR, Warren EP. Electrohydrodynamics of a current-carrying semi-insulating jet. J Fluid Mech 1971;47:127–43.
[11] Ganan-Calvo AM, Davila J, Barrero A. Current and droplet size in the electrospraying of liquids: scaling laws. J Aerosol Sci 1997;28:249.
[12] Ganan-Calvo AM. On the theory of electrohydrodynamically driven capillary jets. J Fluid Mech 1997;335:165–88.
[13] Ganan-Calvo AM. The surface charge in electrospraying: its nature and its universal scaling laws. J Aerosol Sci 1999;30:863–72.
[14] Hayati I, Bailey AI, Tadros TF. Investigation into the mechanisms of electrohydrodynamic spraying of liquids. Effect of electric field and environment on pendant drops and factors affecting the formation of stable jets. J Colloid Interface Sci 1987;117:205–30.
[15] Cherney LT. Electrohydrodynamics of electrified liquid menisci and emitted jets. J Aerosol Sci 1999;30:851–62.
[16] Cherney LT. Structure of Taylor cone jets: limit of low flow rates. J Fluid Mech 1999;378:167–96.
[17] Fernandez de la Mora J, Loscertales IG. The current emitted by highly conducting Taylor cones. J Fluid Mech 1994;260:155–84.
[18] Hohman MM, Shin M, Rutledge G, Brenner MP. Electrospinning and electrically forced jets I: stability theory. Phys Fluids 2001;13: 2201–20.
[19] Hohman MM, Shin M, Rutledge G, Brenner MP. Electrospinning and electrically forced jets II: applications. Phys Fluids 2001;13:2221–36.
[20] Yarin AL, Koombhongse S, Reneker DH. Taylor cone and jetting from liquid droplets in electrospinning of nanofibers. J Appl Phys 2001;90:4836–46.
[21] Feng JJ. The stretching of an electrified non-Newtonian jet: a model for electrospinning. Phys Fluids 2002;14:3912–26.
[22] Yarin AL. Free liquid jets and films: hydrodynamics and rheology. New York: Longman Scientific and Technical; 1993.
[23] MacDiarmid AC, Jones WE, Norris ID, Gao J, Johnson AT, Pinto NJ,

Hone J, Han B, Ko FK, Okuzaki H, Llanguno M. Electrostatically-generated nanofibers of electronic polymers. Synth Met 2001;119: 27–30.

[24] Norris ID, Shaker MM, Ko FK, MacDiarmid AG. Electrostatic fabrication of ultrafine conducting fibers: polyaniline/polyethylene oxide blends. J Synth Metals 2000;114:109–14.

[25] Scopelianos AG. Piezoelectric biomedical device, US patent 5522879, 1996.

[26] Bornat A. A production of electrostatically spun products, US patent 4689186, 1987.

[27] Deitzel JM, Kleinmeyer JD, Hirvonen JK, Beck Tan NC. Controlled deposition of electrospun polyethylene oxide fibers. Polymer 2001;42: 8163–70.

[28] Boland ED, Wnek GE, Simpson DG, Pawlowski KJ, Bowlin GL. Tailoring tissue engineering scaffolds using electrostatic processing techniques: a study of poly(glycolic acid) electrospinning. J Macromol Sci-Pure Appl Chem 2002;A38(12):1231–43.

[29] Zussman E, Theron A, Yarin AL. Formation of nanofiber crossbars in electrospinning. Appl Phys Lett 2003;82(6):973–5.

[30] Bognitzki M, Hou H, Ishaque M, Frese T, Hellwig M, Schwarte C, Schaper A, Wendorff JH, Greiner A. Polymer, metal, and hybrid nano- and mesotubes by coating degradable polymer template fibers (TUFT process). Adv Mater 2000;12(9):636–40.

[31] Dai H-Q, Gong J, Kim H, Lee D. A novel method for preparing ultra-fine alumina-borate oxide fibers via an electrospinning technique. Nanotechnology 2002;13(5):674–7.

[32] Reneker DH, Yarin AL, Evans EA, Kataphinan W, Rangkupan R, Liu W, Koombhongse S, Xu H. Electrospinning and nanofibers, Book of abstracts. New frontiers in fiber science, spring meeting 2001. Available from: http://www.tx.ncsu.edu/jtatm/volume1specialissue/presentations/pres_part1.doc.

[33] Gibson PW, Schreuder-Gibson HL, Riven D. Electrospun fiber mats: transport properties. AIChE J 1999;45(1):190–5.

[34] Jin HJ, Fridrikh S, Rutledge GC, Kaplan D. Electrospinning Bombyx mori silk with poly(ethylene oxide). Abstr Pap Am Chem Soc 2002; 224(1–2):408.

[35] Heinrich R, Bonisch S, Pommerenke D, Jobava R, Kalkner W. Broadband measurement of the conductivity and the permittivity of semiconducting materials in high voltage XLPE cables, 8. Int Conf Dielect Mater Meas Appl Edinburgh, IEE Conf Publ No 473 2000; 212–7.

[36] Stelter M, Brenn G, Yarin AL, Singh RP, Durst F. Validation and application of a novel elongational device for polymer solutions. J Rheol 2000;44:595–616.

[37] Theron A, Zussman E, Yarin AL. Relaxation time measurements of dilute PEO solutions. Internal report 2002-10-Technion-Israel Institute of Technology, 2002.

[38] Saville DA. Electrohydrodynamics, the Taylor Melcher leaky dielectric model. Annu Rev Fluid Mech 1997;29:27–64.

[39] Doshi J, Reneker DH. Electrospinning process and applications of electrospun fibers. J Electrostatics 1995;35:151–60.

[40] Shin YM, Hohman MM, Brenner MP, Rutledge GC. Experimental characterization of electrospinning: the electrically forced jet and instabilities. Polymer 2001;42:9955–67.

[41] Demir MM, Yilgor I, Yilgor E, Erman B. Electrospinning of polyurethane fibers. Polymer 2002;43:3303–9.

[42] Fong H, Reneker DH. Electrospinning nanofibers from polyethylene oxide aqueous solution, Internal report, Maurice Morton Institute of Polymer Science: University of Akron, Ohio 1999.

[43] Baumgarten K. Electrostatic spinning of acrylic microfibers. J Colloid Interface Sci 1971;36(no. 1):71–9.

[44] Doshi J. PhD Dissertation, Akron, Ohio: University of Akron, 1994.

[45] Bockris JOM, Reddy AKN, Modern electrochemistry, vol. 1. New York: Plenum Press; 1970.

[46] Bockris JOM, Reddy AKN, Modern electrochemistry, vol. 2. New York: Plenum Press; 1970.

[47] Reneker DH, Kataphinan W, Theron A, Zussman E, Yarin AL. Nanofiber garlands of polycaprolactone by electrospinning. Polymer 2002;43:6785–94.